processes

Supplementary material

In situ modification of activated carbons by oleic acid under microwave heating to improve adsorptive removal of naphthalene in aqueous solutions

Zhansheng Wu[1,*,a], Pengyun Liu[2,a], Zhilin Wu[2], Giancarlo Cravotto[2,*]

[1] School of Environmental and Chemical Engineering, Xi'an Polytechnic University, Xi'an 710048, China.
[2] Department of Drug Science and Technology, University of Turin, Turin, 10125, Italy; pengyun.liu@edu.unito.it (P.L.); zhilin.wu@unito.it (Z.W.);
* Correspondence: wuzhans@xpu.edu.cn (Z.W.), giancarlo.cravotto@unito.it (G.C.); Tel: +29-83116236 (Z.W.), +39.011.670.7183 (G.C.); Fax: +29-83116236 (Z.W.), +39.011.670.7162 (G.C.)
[a] These authors shared co-first authorship.

Number of pages: 19

Number of figures: 7

Number of tables: 5

Supporting Figures

Section S1. N_2 physisorption isotherms

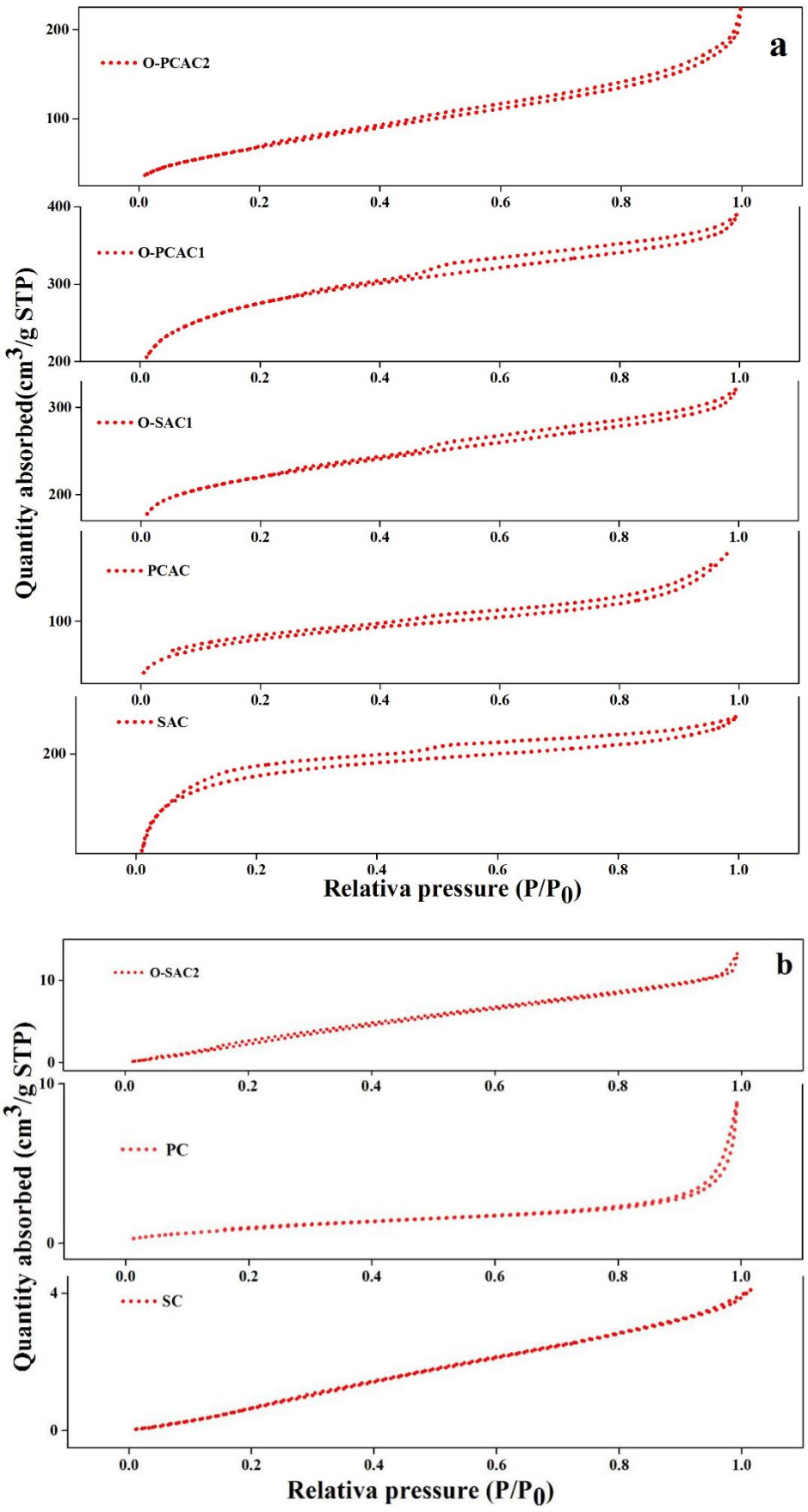

Figure S1. Type I (a) and type II (b) N_2 adsorption/desorption isotherms of samples [19].

Section S2. FTIR analysis

FT-IR results of raw and modified adsorbents are presented in Figure S3a and 3b. The peaks at 3439 and 3445 cm^{-1} were indicative of –OH presence on SC/PC-based adsorbents surface [37]. There are obviously reduced of these two peaks after modification contributed to the replacement of –OH with the oxalate group ($C_{17}H_{33}COO$-) from OA [14]. Three obvious peaks surrounding 3000, 2920, and 2856 cm^{-1} occurred as a result of –CH_2– group stretches associated with C-H bonds [37]. The peak around 2356 cm^{-1} is also caused by –OH stretching, in which O-SAC1, O-PCAC1, and O-PCAC2 show a weaker peak than other adsorbents. This result could contribute to the substitution of –OH by –O–CO– during modification. It has long been known that the appropriate –OH group can increase the adsorption site of the adsorbent surface and lead to an enhancement the adsorption capacity [33]. Nevertheless, the excessive –OH groups can cause the enrichment of acidic groups on adsorbents surface result in low affinity towards non-polar organics (such as NAP). This can be used to understand the low adsorption capacity of PC and O-SAC2 (Figure S2) [21]. The peaks at 1775 cm^{-1} were attributed to the ester and C=O stretching indicates there are polar groups of carboxylic acid, anhydride, O-alkyl, ketone, or ester groups, which lead to low-affinity between adsorbents and NAP. Compared with SAC and PCAC, a weak peak was observed at 1775 cm^{-1} suggested there are a low surface polarity of IMACs and strong adsorption capacity towards NAP [40]. Additional peaks at 1637, 1519, 1469, and 1400 cm^{-1} were assigned to H–O–H bending, C=C of olefinic oil groups, CH_3 and CH_2 alkanes of asymmetric deformation. The broad stretching vibration in the region of 1236−1081 cm^{-1} was owing to C–O stretching of carboxylic by changing the bond length and bond angle resulted from the formation of hydrogen bonds between adsorbents and OA [15, 37, 41]. Low-intensity peaks at 1375 cm^{-1} can be attributed to a CH_3 symmetric deformation

caused by the introduction of oil acid [12]. Peaks ~808 cm^{-1} associated with C–H out of plane-vibration of alkenes in oleate [15].

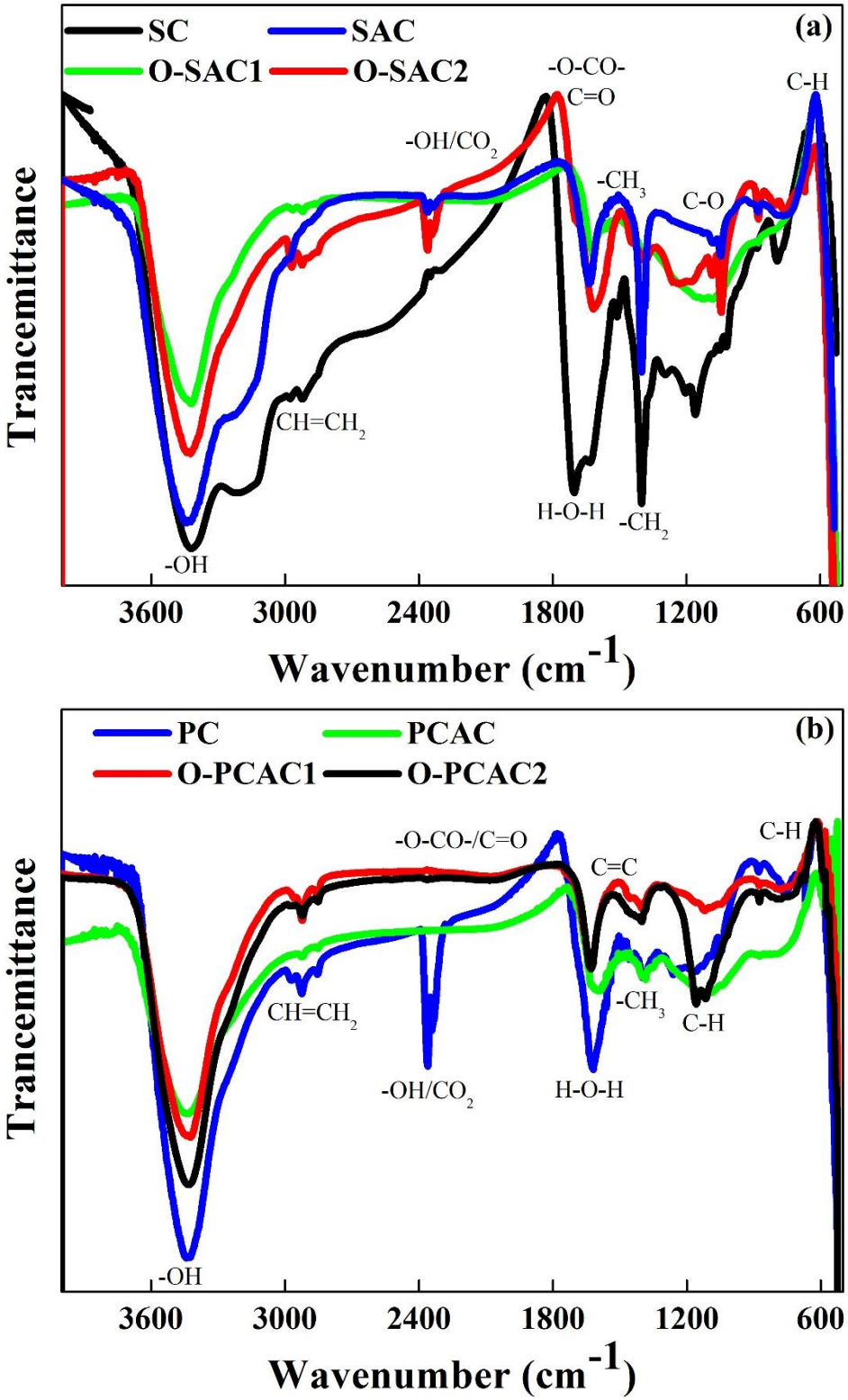

Figure S2. FTIR spectra of SC-based (a) and PC-based (b) samples [19].

Section S3. SEM images

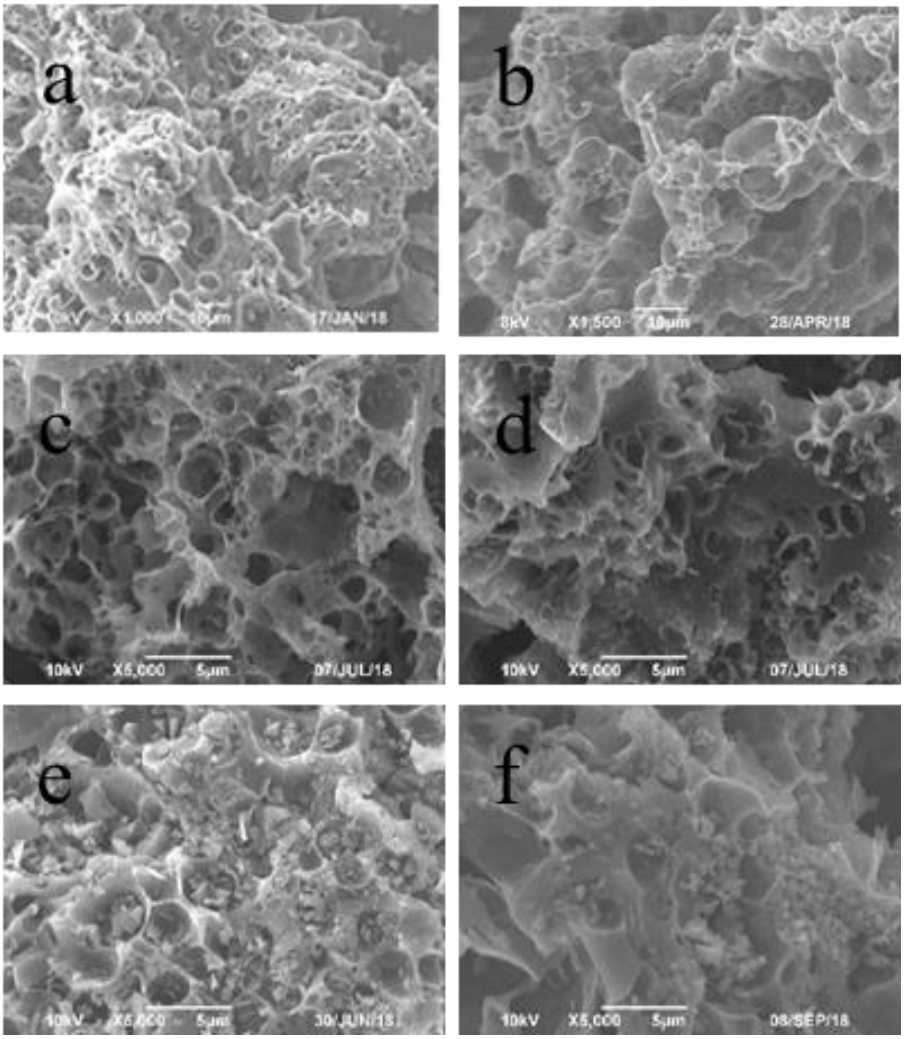

Figure S3. Morphological images of PCAC (a), SAC (b), O-PCAC1 (c), O-SAC1 (d), O-PCAC2 (e) and O-SAC2 (f) [19].

Section S4. Adsorption kinetics

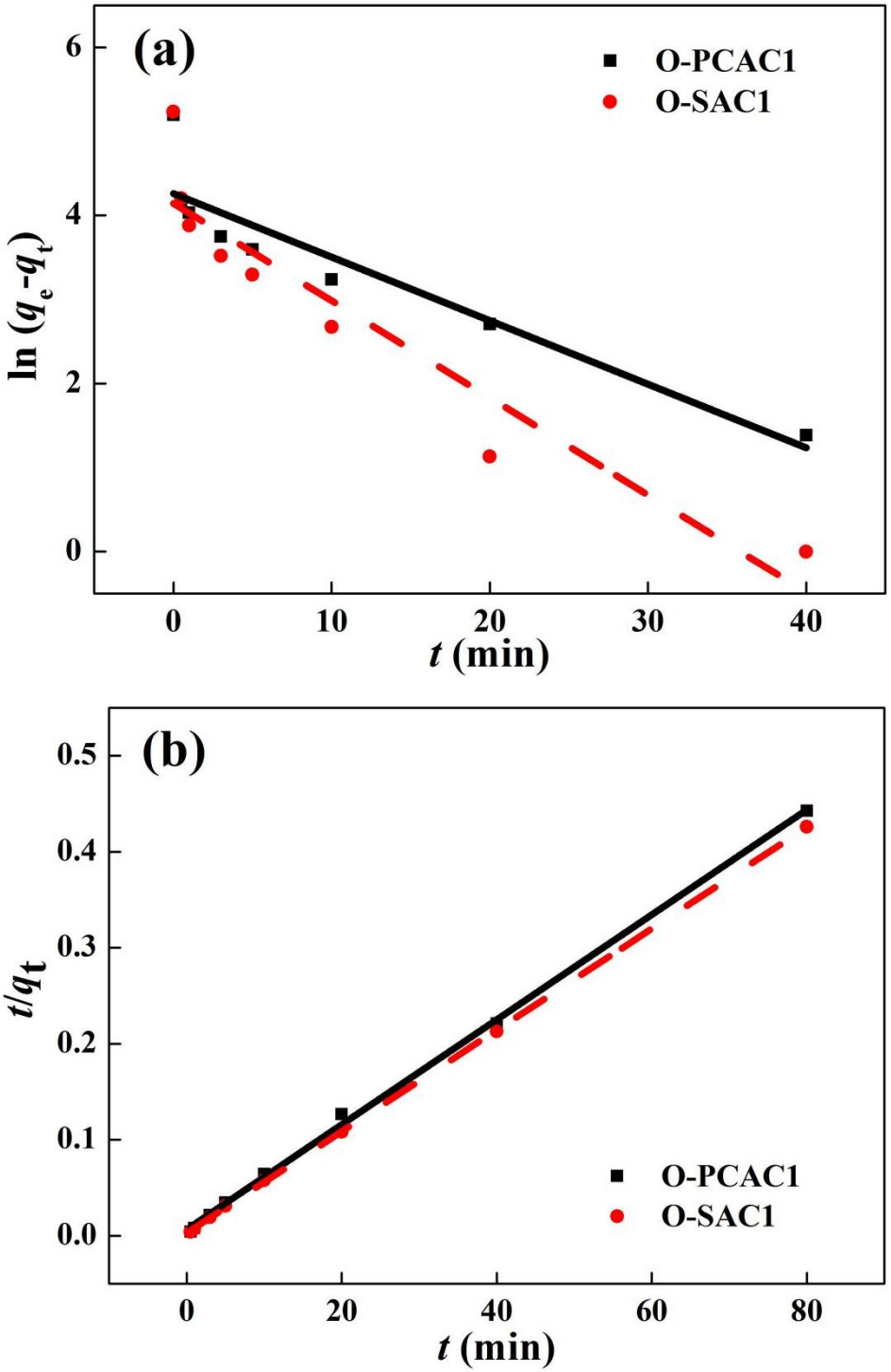

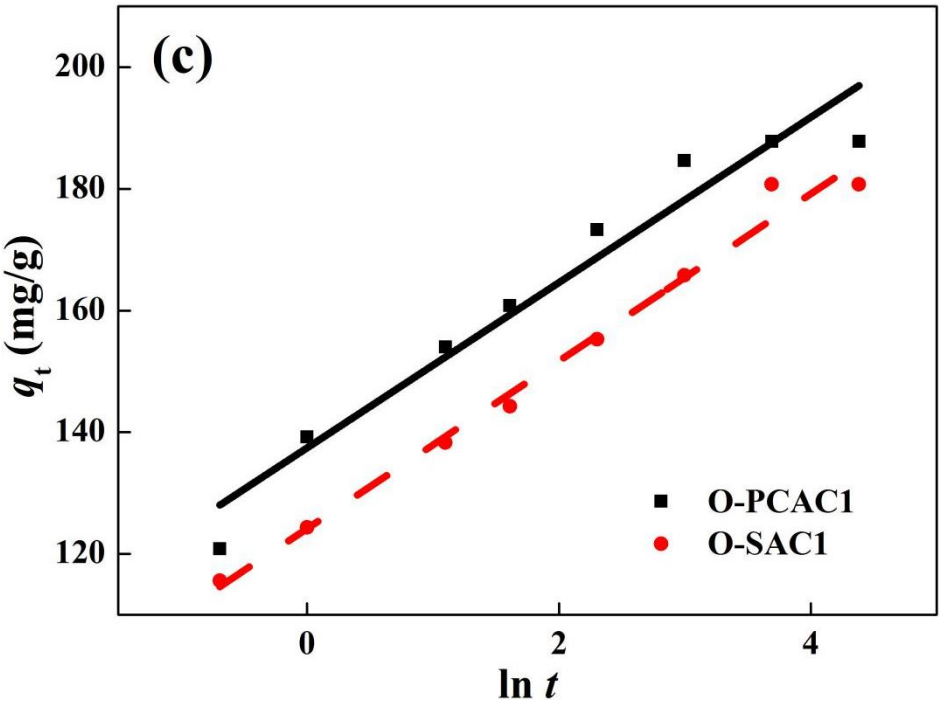

Figure S4. The fit of kinetic data concerning IMACs adsorption towards NAP by pseudo-first-order (a), pseudo-second-order (b), and Elovich kinetic models (c).

Section S5. Adsorption isotherm

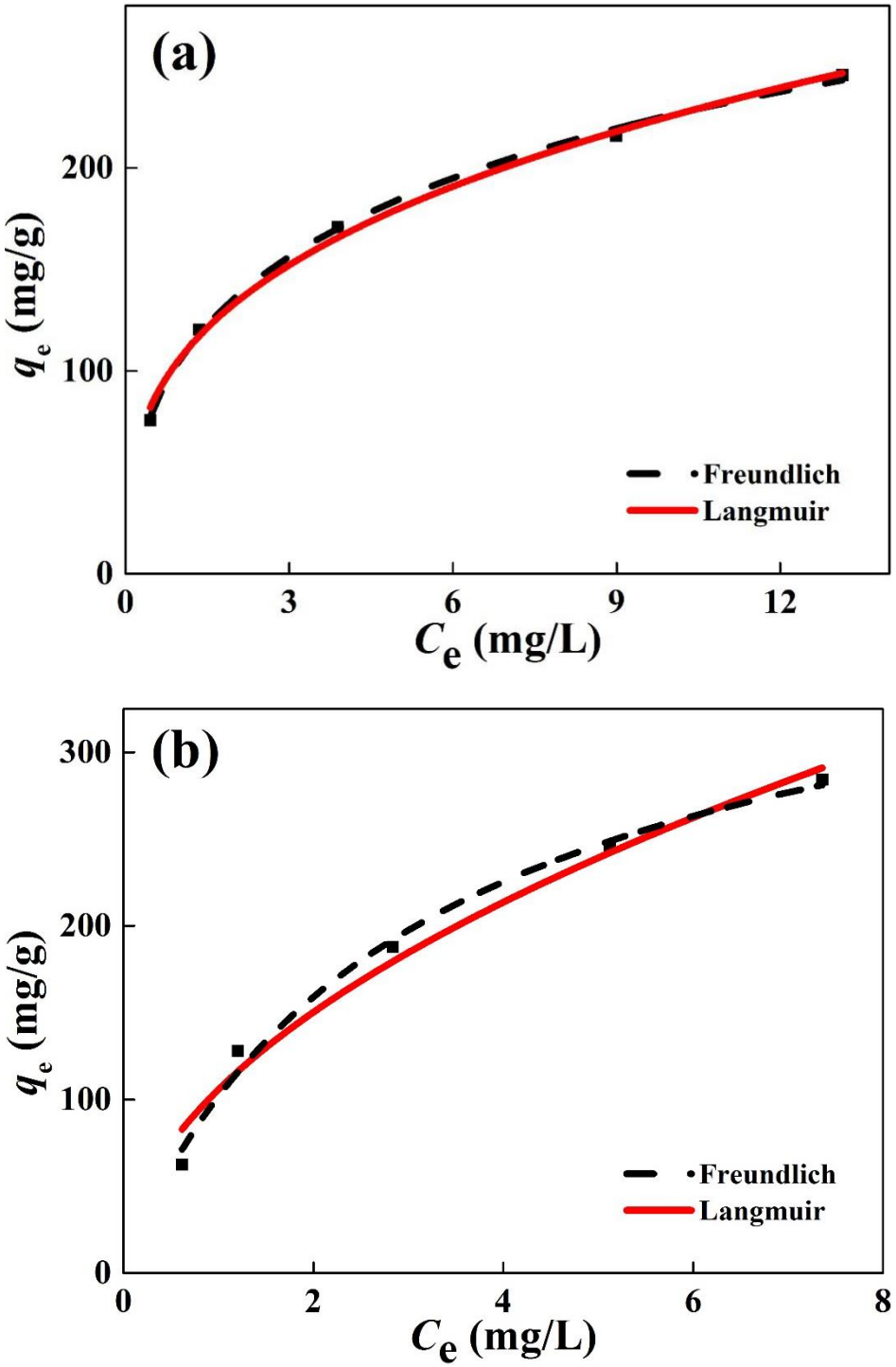

Figure S5. Equilibrium adsorption isotherms of NAP on O-SAC1 (a) and O-PCAC1 (b) at 303 K.

Section S6. Adsorption mechanism

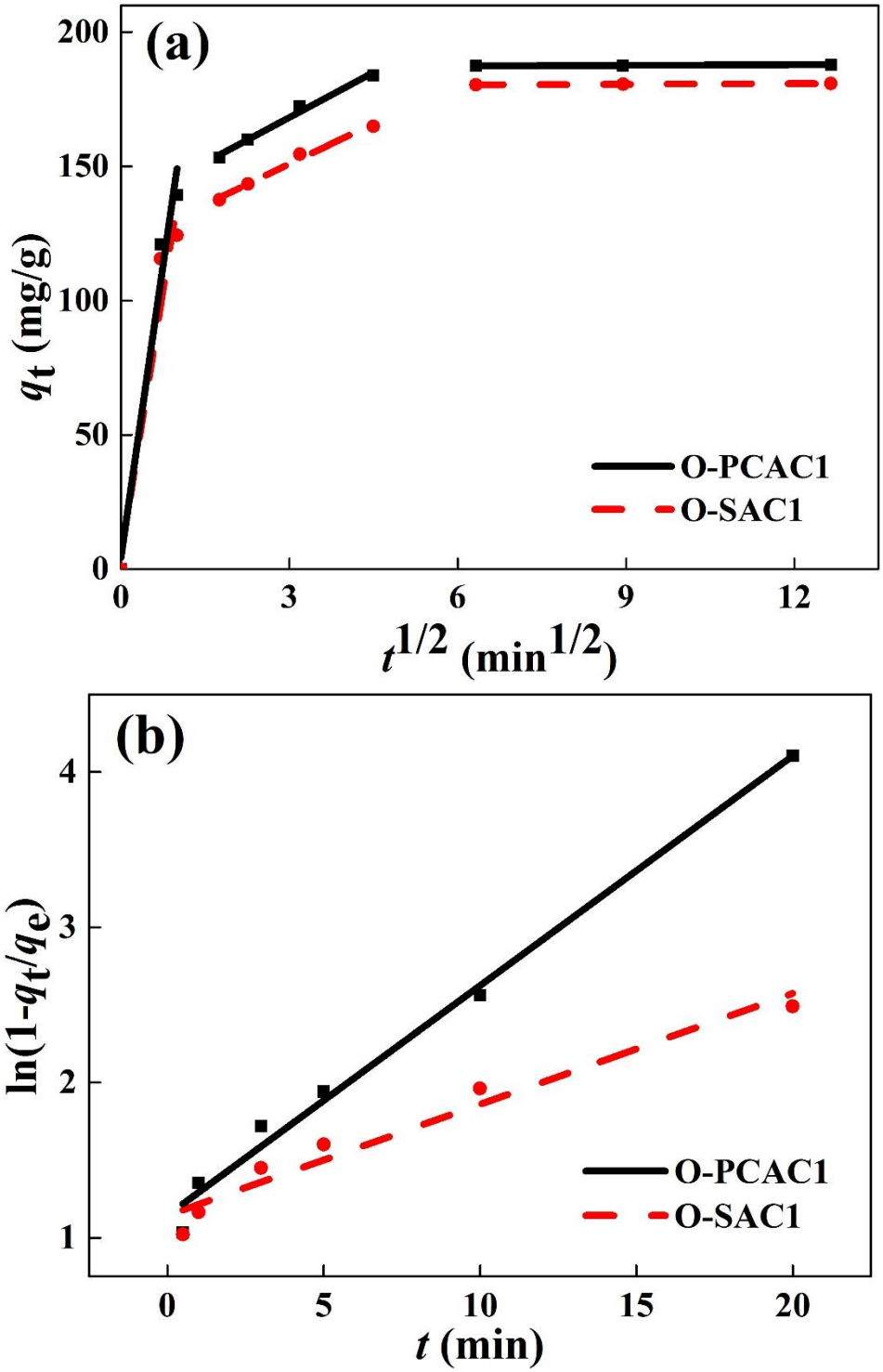

Figure S6. Intraparticle diffusion (a) and film diffusion (b) models for the adsorption of NAP on IMACs at 303 K.

Section S7 Effect of solution pH

The initial pH can influence the adsorption performance by controlling the surface charges and ionization level of the adsorbent-adsorbate system [35]. The pH (measured with a PHS-3c pH meter, Shanghai, China) of the solutions was adjusted to 2-10 using 0.1 M sodium hydroxide and 0.1 M hydrochloric acid to evaluate the pH effect on NAP adsorption using IMACs at the initial concentration of 30 mg/L.

Figure S7 describes the effect of solution pH on NAP adsorption onto IMACs. As observed, the NAP adsorption inconspicuously changed with varying pH in both cases. This limited effect is likely to be associated with the O-containing groups in adsorbents that acted as a buffer during the adsorption. Furthermore, O-containing groups could interact with both H^+ and OH^- ions through the protonation of O atoms by H^+ and the formation of H-bond between O atoms and OH^-. A similar observation was reported by Wei et al. in the removal of atrazine using ACs from water [34].

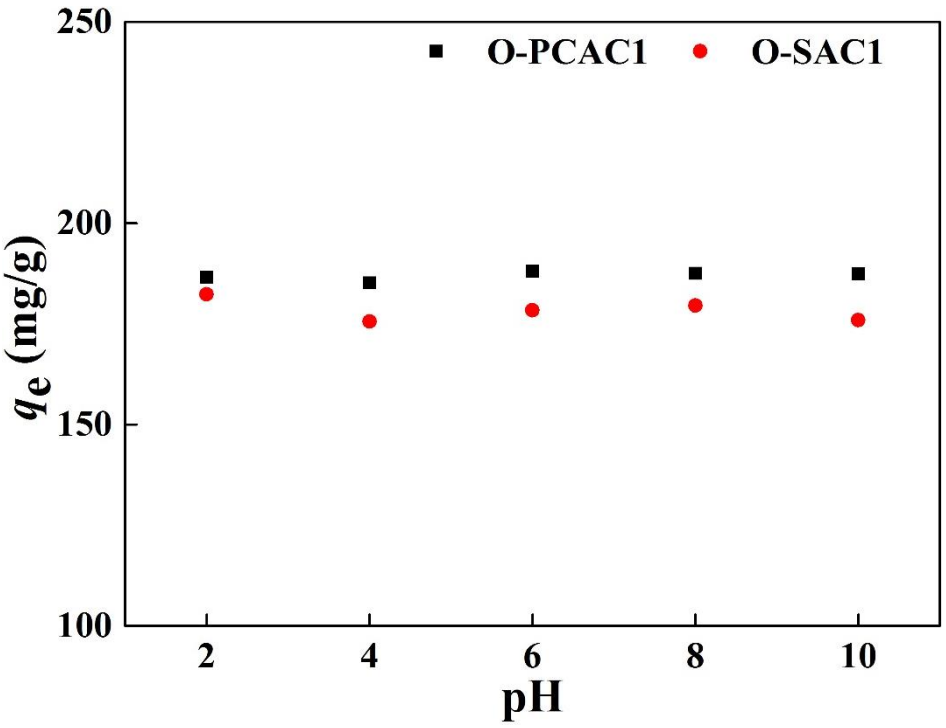

Figure S7. Influence of initial pH on NAP adsorption on IMACs (NAP concentration 30 mg/L, contact time 80 min).

Supporting Tables

Section S1. Functional groups on raw and modified samples

Table S1 Functional groups on raw and modified samples, according to FTIR analysis.

Wavenumber (cm^{-1})	Functional groups	SC	PC	SAC	PCAC	O-SAC1	O-SAC2	O-PCAC1	O-PCAC2
3439/3445	–OH	√	√	√	√	√	√	√	√
3000/2920/2856	$CH{=}CH_2$	√	√	–	–	√	√	√	√
2356/2365	$–OH/CO_2$	–	√	–	–	–	√	–	–
1775/1778	–O–CO–/C=O	√	√	√	√	√	√	–	–
1637/1602	H–O–H	√	√	√	√	√	√	√	√
1519	C=C(OA)	–	√	–	√	–	–	√	√
1469	$–CH_3$	√	–	√	–	√	√	–	–
1400	$–CH_2$	√	–	√	–	√	√	–	–
1379	$–CH_3$	–	√	–	√	–	–	√	√
1080-1236	C–O	√	–		–	√	√	–	–
1170/913/621	C–H	√	√	√	√	√	√	√	√
Note: √ (present), - (not present).									

Section S2. Adsorption models

The pseudo-first-order (PFO), pseudo-second-order (PSO) and Elovich kinetic models; the Langmuir, Freundlich isotherm models; and intraparticle diffusion, film diffusion models were used to interpret the adsorption process of naphthalene (NAP) on *in situ* modified ACs (IMACs) [12, 15, 35]. And the Thomas and Adams–Bohart dynamic adsorption models were used to fit the fixed bed column experimental data [27]. The model expressions and explanations are summarized in Table S2. The residual root-mean-squared-error function values (*RMSE*) and correlation coefficients (R^2) were determined by adopting Eq. (S1) and (S2):

$$RMSE=\left[\sum_{N=1}^{N}\left(q_{e,exp}-q_{e,cal}\right)^2/(N-1)\right]^{1/2} \quad (S1)$$

$$R^2=1-\sum_{N=1}^{N}\left(q_{e,exp,N}-q_{e,cal,N}\right)^2/\sum_{N=1}^{N}\left(q_{e,exp,N}-\overline{q_{e,exp,N}}\right)^2 \quad (S2)$$

Note: $q_{e,exp}$ and $q_{e,cal}$ are the experimental and calculated values for q_e, respectively. N represents the number of experiments. The experimental data were analyzed using origin 9.0.

Table S2 Adsorption models for naphthalene removed by O-SAC1 and O-PCAC1 [12, 15, 27, 35].

Models	**Equation**	**Nomenclature**
PFO	$\ln\left(q_e-q_t\right)=\ln q_e-\frac{K_1}{2.303}t$	(q_t, mg/g) – adsorption capacity at any point of time t (K_1, 1/min) – pseudo-first-order rate constant
PSO	$\frac{t}{q_t}=\frac{1}{K_2 q_e^{\ 2}}+\frac{t}{q_e}$	(K_2, g/(mg min)) – pseudo-second-order rate constant
Elovich	$q_t=\frac{1}{\beta}\ln\left(\alpha\beta\right)+\frac{1}{\beta}\ln(t)$	(α, mg/(g min)) – initial sorption constant (β, g/mg) – initial desorption constant
Langmuir	$\frac{C_e}{q_e}=\frac{1}{q_m}C_e+\frac{1}{q_m K_L}$	(q_m, mg/g) –the maximal adsorption capacity (K_L, L/mg) – a constant related to the free energy
Freundlich	$q_e=K_F C_e^{\frac{1}{n}}$	(K_F, L/mg) – a constant related to the bonding energy ($1/n$) – a constant related to adsorption intensity
Intraparticle diffusion	$q_t=K_P t^{\frac{1}{2}}+C$	(K_P, mg/(g min$^{1/2}$)) – the intraparticle diffusion constant C – a constant related to the boundary layer thickness
Film diffusion	$-\ln\left(1-\frac{q_t}{q_e}\right)=K_{bf}\,t$	(K_{bf}, 1/min) – liquid-film diffusion constant

Thomas	$\frac{C_t}{C_0}=\frac{1}{1+\exp\left(\frac{k_{Th}q_0 m}{v}-k_{Th}C_0 t\right)}$	(k_{Th}, mL/(min mg)) – the Thomas rate constant (q_0, mg/g) – the adsorption capacity (v, mL/min) – the feed flow rate
Adam's–Bohart	$\frac{C_t}{C_0}=\exp\left(k_{AB}C_0 t-k_{AB}N_0\frac{z}{U_0}\right)$	(k_{AB}, L/(mg min)) – the kinetic constant (N_0, mg/L) – the saturation concentration (z, cm) – the bed depth of the fixed bed column (U_0, cm/min) – the superficial velocity

Section S3. Adsorption mechanism

Table S3 Intraparticle- and film-diffusion parameters of IMACs at 303 K.

Models	Parameters	O-SAC1	O-PCAC1
Intraparticle diffusion	K_{p1} (mg/g min$^{1/2}$)	131.57	145.12
	K_{p2} (mg/g min$^{1/2}$)	10.04	11.20
	K_{p3} (mg/g min$^{1/2}$)	0.0792	0.0795
	$(R_1)^2$	0.8998	0.9448
	$(R_2)^2$	0.9809	0.9841
	$(R_3)^2$	0.9995	0.9991
Film diffusion	K_{bf} (1/min)	0.0715	0.1480
	R^2	0.9462	0.9872

Section S4. Column adsorption models

Table S4 Column adsorption models fitting of NAP adsorption on O-SAC1.

Thomas				O-SAC1			
Z cm	Q_0 mL/min	C_0 mg/L	D cm	A cm^2	K_{Th} mL/(mg min)	$q_{e,cal}$ (mg/g)	R^2
1	2	30	3.38	8.97	0.00136	621.30	0.9839
2	2	30	3.38	8.97	0.00128	501.49	0.9822
3	2	30	3.38	8.97	0.00125	455.76	0.9109
1	1	30	3.38	8.97	0.00117	796.67	0.9505
1	3	30	3.38	8.97	0.00194	434.18	0.9863
1	2	10	3.38	8.97	0.00310	315.03	0.9654
1	2	20	3.38	8.97	0.00178	495.08	0.9745
Adams-Bohart				O-SAC1			
Z cm	Q_0 mL/min	C_0 mg/L	D cm	A cm^2	k_{AB} L/(mg min)	N_0 mg/L	R^2
1	2	30	3.38	8.97	0.00042	325.57	0.8586
2	2	30	3.38	8.97	0.00030	289.26	0.8112
3	2	30	3.38	8.97	0.00034	229.60	0.8922
1	1	30	3.38	8.97	0.00043	241.83	0.9233
1	3	30	3.38	8.97	0.00063	294.73	0.8913
1	2	10	3.38	8.97	0.00107	147.94	0.9041
1	2	20	3.38	8.97	0.00059	245.42	0.8962

Table S5 Column adsorption models fitting of NAP adsorption on O-PCAC1.

Thomas				O-PCAC1			
Z	Q_0	C_0	D	A	K_{Th}	$q_{e,cal}$	R^2
cm	mL/min	mg/L	cm	cm²	mL/(mg min)	mg/g	
1	2	30	3.38	8.97	0.00086	1398.76	0.9545
2	2	30	3.38	8.97	0.00066	1218.15	0.9666
3	2	30	3.38	8.97	0.00063	1156.70	0.9107
1	1	30	3.38	8.97	0.00076	1444.61	0.9033
1	3	30	3.38	8.97	0.00221	917.60	0.9309
1	2	10	3.38	8.97	0.00294	580.07	0.9193
1	2	20	3.38	8.97	0.00108	1168.06	0.9701
Adams-Bohart				O-PCAC1			
Z	Q_0	C_0	D	A	k_{AB}	N_0	R^2
cm	mL/min	mg/L	cm	cm²	L/(mg min)	mg/L	
1	2	30	3.38	8.97	0.00029	628.35	0.8728
2	2	30	3.38	8.97	0.00023	603.59	0.8735
3	2	30	3.38	8.97	0.00025	557.98	0.9022
1	1	30	3.38	8.97	0.00026	461.27	0.7763
1	3	30	3.38	8.97	0.00066	389.56	0.8949
1	2	10	3.38	8.97	0.00074	284.34	0.8719
1	2	20	3.38	8.97	0.00042	484.96	0.9064

References

12. Younis, S.A.; El-Sayed, M.; Moustafa, Y.M. Modeling and optimization of oil adsorption from wastewater using an amorphous carbon thin film fabricated from wood sawdust waste modified with palmitic acid. *Environ. Process*. **2017**, *4*, 147-168.
14. Sathasivam, K.; Haris, M.R.H.M. Adsorption kinetics and capacity of fatty acid-modified banana trunk fibers for oil in water. *Water Air Soil Poll*. **2010**, *213*, 413-423.
15. Zhu, M.; Yao, J.; Dong, L.; Sun, J.J. Adsorption of naphthalene from aqueous solution onto fatty acid modified walnut shells. *Chemosphere*. **2016**, *144*, 1639-1645.
19. Liu, P.Y.; Wu, Z.S.; Sun, Z.H.; Ye, J. Comparison study of naphthalene adsorption on activated carbons prepared from different raws. *Korean J. Chem. Eng.* **2018**, *35*, 2086-2096.
20. Liu, P.Y.; Wu, Z.S.; Ge, X.Y.; Yang, X. Hydrothermal synthesis and microwave-assisted activation of starch-derived carbons as an effective adsorbent for naphthalene removal. *RSC. Advance.* **2019**, *9*, 11696-11706.
21. Ge, X.Y.; Tian, F.; Wu, Z.S.; Yan, Y.J.; Cravotto, G.; Wu Z.L. Adsorption of naphthalene from aqueous solution on coal-based activated carbon modified by microwave induction: Microwave power effects. *Chem. Eng. Process*. **2015**, *91*, 67-77.
27. Auta, M.; Hameed, B.H. Acid modified local clay beads as effective low-cost adsorbent for dynamic adsorption of methylene blue. *J. Ind. Eng. Chem.* **2013**, *19*, 1153-1161.
33. Niazi, L.; Lashanizadegan, A.; Sharififard, H. Chestnut oak shells activated carbon: Preparation, characterization and application for Cr (VI) removal from dilute aqueous solutions. *J. Clean. Prod.* **2018**, *185*, 554-561.
34. Wei, X.H.; Wu, Z.S.; Wu, Z.L.; Ye, B.C. Adsorption behaviors of atrazine and Cr (III) onto different activated carbons in single and co-solute systems. *Powder Technol.* **2018**, *329*, 207-216.
35. Ghaedi, M.; Daneshyar, A.; Asfaram, A.; Purkait, M.K. Adsorption of naphthalene onto high-surface-area nanoparticle loaded activated carbon by high performance liquid chromatography: response surface methodology, isotherm and kinetic study. *RSC. Adv.* **2016**, *6*, 54322-54330.
37. Norouzi, S.; Heidari, M.; Alipour, V.; Rahmanian, O.; Fazlzadeh, M. Mohammadi-Moghadam, F, Nourmoradi, H, Goudarzi, B, Dindarloo, K. Preparation, characterization and Cr (VI) adsorption evaluation of NaOH-activated carbon produced from Date Press Cake; an agro-industrial waste. *Bioresource Technol.* **2018**, *258*, 48-56.
40. Liu, N.; Charrua, A.B.; Weng, C.H.; Yuan, X.L.; Ding, F. Characterization of biochars derived from agriculture wastes and their adsorptive removal of atrazine from aqueous solution: A comparative study. *Bioresource Technol.* **2015**, *198*, 55-62.
41. Liu, Y.J.; Ying, D.Y.; Sanguansri, L.; Cai, Y.X.; Le, X.Y. Adsorption of catechin onto cellulose and its mechanism study: Kinetic models, characterization and molecular simulation. *Food Res. Int.* **2018**, *112*, 225-232.